IRAQI Academic Scientific Journals
Samarra Journal of Pure and Applied Science
SJPAS
www.sjpas.com
p ISSN: 2663-7405
e ISSN: 2789-6838

Effect of Double-Diffusive Stagnation point flow of Eyring– Powell Nanofluid on a Slender Stretching Sheet with Non-uniform heat Source Sink and Inclined Magnetic Field

Asha S. K.* and Gayitri Mali
Department of Mathematics, Karnatak University, Dharwad – 580003, Karnataka, India
https://doi.org/10.54153/sjpas.2023.v5i1.435

Article Information
Received: 29/11/2022
Accepted: 28/02/2023
Keywords:
Slender Stretching Sheet, Stagnation point flow, Non-uniform Heat Source Sink, Eyring-Powell Nanofluid.

Corresponding Author
E-mail: ashask@kud.ac.in
Mobile:

Abstract
In the present paper, the effects of an inclined magnetic field and a non-uniform heat source sink on a double diffusive convective stagnation point flow in a slender stretching sheet are studied. The suitable similarity transformation is utilized for the conversion of nonlinear differential equations. These converted equations are solved by means of Differential Transformation method (DTM) with the support of symbolic software Mathematica. Further, the effects of appropriate parameters on velocity profile, solute, nanoparticle concentration and temperature profiles are shown graphically with some suitable discussions. It is found that velocity decreases with a rise of magnetic parameter. Because applying the uniform magnetic field normal to the flow direction gives rise to Lorentz force. This force has the tendency to slow down the velocity of the fluid in the boundary layer. Also non-uniform heat source sink parameters enhance the thermal profile of the system. But, opposite behavior can be seen in solute and nanoparticle concentration profiles. Such results can be useful in design and structure of materials, where implementation of variable thickness decreases the weight of stretched element and boosts the usage of materials.

1. INTRODUCTION:

In various industrial and engineering processes, prominent importance of boundary layer flow over stretching sheet can be seen. For instance, in polymer sheets extrusion, production of glass-fiber and paper, wire drawing, metal-spinning. The theory of boundary layer flow on a stretching sheet with linear stretching velocity was coined by Crane [1]. After his work, several researchers gave their attention towards the flow over stretching surface with linear stretching velocity [2-4], nonlinear stretching velocity [5-7] and exponential stretching velocity [8-10]. In the above cited literature, the stretching sheet with uniform thickness is taken. But slender stretching sheet (Stretching sheet with variable thickness) looks more practical compared to flat stretching sheet. Especially, in civil engineering, mechanical, aeronautical design, the applications of variable thickness sheet can be seen. It assists to decrease the weight of structural

elements and boosts the usage of material. Thought of slender stretching sheet was originated by Lee [11]. Boundary layer flow of a continuously stretched sheet with changing thickness was studied by Fang et al. [12]. Later, Reddy et al. [13] explored idea of the effect of variable thickness and variable temperature profile over flat stretching sheet. Whereas, Khader et al. [14] extended the work of variable thickness over non-linear stretching sheet for slip velocity.

The stream of a non-Newtonian fluid at lower pressure due to stretching sheet finds its applications in engineering process. The continuous flow of a fluid near a solid surface is usually referred as stagnation point flow. When fluid tends towards the surface, it divides into two streams. At the point of stagnation, the fluid pressure, the heat transfer and the rate of mass accumulation is very high. Due to this fact, many researchers diverted their interest towards this. Mahapatra et al. [16] analyzed the thermal conduction phenomenon in a stagnation point flow when stretching velocity is lesser than a free stream velocity. The analysis of heat transfer on stagnation point flow over a inclined cylinder and exponentially stretching sheet for Eyring-Powell fluid model and micropoloar fluid is studied by Rehmana et al. [17, 18]. Further, Vinod et al. [19] explored the stagnation point flow in a slender stretching sheet by considering nanofluid model. Researcher found that boundary layer formation is similar even though the stretching velocity is more than a free steam velocity. Stagnation point flow for different geometry of stretching sheet is given in ref. [20-22].

Impact of heat source sink on heat transfer cannot be ignored for double diffusive convective flow and also for the stability of fluid motion. Variation of heat distribution in the fluid can be seen by heat generation or absorption and also impacts the particle accumulation. Bhuvanavijaya et al. [23],Venkateswarlu et al. [24] andSugunamma et al. [25] demonstrated the effect of non-uniform heat source sink in different geometry by considering Newtonian fluids. The viscous fluid of non-Newtonian fluid has gain lot of attention due to its extensive industrial and technical applications. This particular fluid model is obtained from the kinetic theory of liquids and also it shows Newtonian behavior at high and low shear rates. Further some other studies on Eyring-Powell fluid are given in [26-29].

No attempt has been made in any of the previously stated investigations to consider the combined effects of all of the aforementioned parameters. Our key interest and novelty of this present investigation is to examine how the double diffusion convective stagnation-point flow and Eyring-Pwell nanofluid effects on slender stretching sheet under the impact of non-uniform heat source sink and angled magnetic field. The present analysis has wide applications in design and structure of materials.Some researchers began studying double diffusive convection in nanofluids a few years ago, and it has remained interesting due to its wide variety of applications in water saturated soils.In fluid mechanics, equations are involved are non-linear differential equations. It's difficult to come up with accurate answers to such equations. There has been an increase in attention to developing and utilizing analytical and numerical methodologies. In current article we applied Differential Transform Method (DTM) to solve non-linear differential equations. The differential transformation method (DTM) is used to solve directly to nonlinear ODE without the need of initial guess or discretization and it is unaffected by discretization

mistakes [30-32]. The effects of appropriate parameters on velocity profile, solute concentration, nanoparticle concentration and temperature profiles are shown graphically with some suitable discussion.

2. MATHEMATICAL FORMULATION

The velocity of a stretching sheet as well as the velocity of the free stream are $U_w(x)=U_0(x+b)^m$ and $U_e(x)=U_1(x+b)^m$.The non-flat sheet equation is given as $y=E(x+b)^{\frac{1-m}{2}}$ $(m\neq 1)$, E is a constant therefore the sheet is enough thin to ignore $\frac{\partial p}{\partial x}=0.$

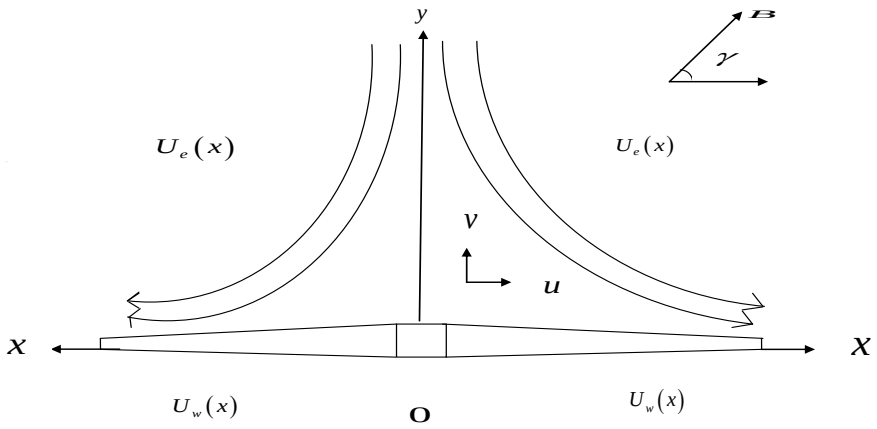

Fig.1 Schematic Geometry of the flow model

2.1 Fluid Model

The stress tensor in Eyring-Powel model

$$\rho_{ij}=\mu\frac{\partial u_i}{\partial x_j}+\frac{1}{\beta}\sinh^{-1}\left(\frac{1}{c_*}\frac{\partial u_i}{\partial x_j}\right), \tag{1}$$

$$\sinh^{-1}\left(\frac{1}{c_*}\frac{\partial u_i}{\partial x_j}\right)\cong\frac{1}{c_*}\frac{\partial u_i}{\partial x_j}-\frac{1}{6}\left(\frac{\partial u_i}{\partial x_j}\right)^3,\left|\frac{1}{c_*}\frac{\partial u_i}{\partial x_j}\right|<1, \tag{2}$$

where β and c_* are Erying-Powell rheological fluid parameters.

From the above mentioned assumptions the governing equations are [12, 22, 23, 24, 25, 28]

$$\frac{\partial u}{\partial x}+\frac{\partial v}{\partial y}=0, \tag{3}$$

$$u\frac{\partial u}{\partial x}+v\frac{\partial u}{\partial y}=U_e\frac{\partial U_e}{\partial x}+\left(\upsilon+\frac{1}{\rho_f\beta c_*}\right)\frac{\partial^2 u}{\partial y^2}-\frac{1}{2\rho_f\beta c_*{}^3}\left(\frac{\partial u}{\partial y}\right)^2\frac{\partial^2 u}{\partial y^2}+$$
$$\left[\begin{array}{l}(1-C_\infty)\rho_f\beta_T g(T-T_\infty)+(1-C_\infty)\rho_f\beta_{C_1} g(C_1-C_{1\infty})-\\ (\rho_p-\rho_f)g(C-C_\infty)\end{array}\right]- \tag{4}$$
$$\frac{\sigma B_0{}^2(x+b)^{m-1}}{\rho_f}(u-U_e)\sin^2\gamma,$$

$$u\frac{\partial T}{\partial x}+v\frac{\partial T}{\partial y}=\alpha\frac{\partial^2 T}{\partial y^2}+\tau\left[D_B\frac{\partial C}{\partial y}\frac{\partial T}{\partial y}+\frac{D_T}{T_\infty}\left(\frac{\partial T}{\partial y}\right)^2\right]+D_{TC_1}\frac{\partial^2 C_1}{\partial y^2}+\frac{q'''}{(\rho C_p)_f}, \tag{5}$$

$$u\frac{\partial C_1}{\partial x}+v\frac{\partial C_1}{\partial y}=D_{S_1}\frac{\partial^2 C_1}{\partial y^2}+D_{C_1T}\frac{\partial^2 T}{\partial y^2}, \tag{6}$$

$$u\frac{\partial C}{\partial x}+v\frac{\partial C}{\partial y}=D_B\frac{\partial^2 C}{\partial y^2}+\frac{D_T}{T_\infty}\frac{\partial^2 T}{\partial y^2}. \tag{7}$$

Where, u and v are velocity components along x and y directions, respectively. μ is the coefficient of fluid viscosity, ρ_f is density of the fluid, g is the gravitational acceleration, ρ_p is density of the particles, β_T is fluid's volumetric thermal expansion coefficient, B_0 is magnetic field strength, σ is the electrical conductivity, β_{C_1} is volumetric solutal expansion coefficient, T is the temperature of the fluid, C is nanoparticle concentration, C_1 is solutal concentration, $\alpha=\frac{k}{(\rho c)_f}$ is thermal diffusivity, υ is kinematic viscosity, D_B is Brownian diffusion coefficient, τ is ratio of effective heat capacity of the nanoparticle material to heat capacity of the fluid, D_{TC_1} is Doufertype diffusivity, D_{S_1} is solutal diffusivity, D_{C_1T} is Soret type diffusivity.

The boundary conditions [12, 13, 17]

$$u=U_w(x)=U_0(x+b)^m,\quad v=0,\quad T=T_w,\quad C=C_w,\quad C_1=C_{1w}\ \ at\ y=E(x+b)^{\frac{1-m}{2}} \tag{8}$$

$$u\to U_e,\quad T\to T_\infty,\quad C\to C_\infty,\quad C_1\to C_{1\infty,}\ \ at\ y\to\infty. \tag{9}$$

The non-uniform heat source sink represented as [22, 23]

$$q'''=\frac{kU_w}{\upsilon(x+b)}\left(A^*(T_w-T_\infty)F'+B^*(T-T_\infty)\right). \tag{10}$$

Similarity transformations are:

$$\left.\begin{aligned} &u = U_0(x+b)^m F'(\eta),\ v = -\sqrt{\frac{m+1}{2}\upsilon U_0(x+b)^{m-1}}\left[F(\eta)+\eta F'(\eta)\left(\frac{m-1}{m+1}\right)\right], \\ &\Theta(\eta) = \frac{T-T_\infty}{T_w-T_\infty},\ \Phi(\eta) = \frac{C-C_\infty}{C_w-C_\infty},\ \mathrm{X}(\eta) = \frac{C_1-C_{1\infty}}{C_{1w}-C_{1\infty}},\ \eta = y\sqrt{\frac{m+1}{2}\frac{U_0(x+b)^{m-1}}{\upsilon}}. \end{aligned}\right\} \quad (11)$$

Where $\psi(x,y)$ is:

$$u = \frac{\partial\psi}{\partial y},\quad v = -\frac{\partial\psi}{\partial x} \quad (12)$$

Equation (3) is automatically satisfied by using (11) and equations (3) - (7) are reduced into ordinary differential equations:

$$\begin{aligned} &(1+N)F''' + FF'' - \frac{2m}{m+1}(F')^2 - N\delta\left(\frac{m+1}{2}\right)F'''(F'')^2 + \frac{2m}{m+1}A^2 - \\ &\frac{2}{m+1}M^2\sin^2(\gamma)(F'-A) + \frac{2}{m+1}\lambda(\Theta + Nc\mathrm{X} - Nr\Phi) = 0, \end{aligned} \quad (13)$$

$$\Theta'' + \Pr\left(F\Theta' + Nb\Theta'\Phi' + Nt(\Theta')^2 + Nd\,\mathrm{X}''\right) + \frac{2}{m+1}\left(A^*F' + B^*\Theta\right) = 0, \quad (14)$$

$$\mathrm{X}'' + Sc\,F\,\mathrm{X}' + Ld\,\Theta'' = 0, \quad (15)$$

$$\Phi'' + Sc_n F\,\Phi' + \frac{Nt}{Nb}\Theta'' = 0. \quad (16)$$

Boundary conditions (8) and (9) are transformed as follows,

$$\left.\begin{aligned} &F(\Omega) = \frac{\Omega(1-m)}{(1+m)},\ F'(\Omega) = 1,\ \Theta(\Omega) = 1,\ \Phi(\Omega) = 1,\ \mathrm{X}(\Omega) = 1, \\ &F'(\infty) = A,\ \Theta(\infty) = 0,\ \Phi(\infty) = 0,\ \mathrm{X}(\infty) = 0. \end{aligned}\right\} \quad (17)$$

Primes signify the differentiation with regard to η from the above mentioned statements.

Where, $\Omega = E\sqrt{\frac{m+1}{2}\frac{U_0}{\upsilon}}$ represents wall thickness parameter and $\eta = \Omega = E\sqrt{\frac{m+1}{2}\frac{U_0}{\upsilon}}$ shows the plate surface.

Equations (13) - (16) along with equation (17) are with a domain $[\Omega,\infty)$.To make the calculation easier to understand, convert $[\Omega,\infty)$ into $[0,\infty)$ and we represent f, θ, χ and ϕ as,

$$F(\eta) = f(\eta-\Omega) = f(\xi),\ \Theta(\eta) = \theta(\eta-\Omega) = \theta(\xi),\ \mathrm{X}(\eta) = \chi(\eta-\Omega) = \chi(\xi),\ \Phi(\eta) = \phi(\eta-\Omega) = \phi(\xi)$$

So equations (13) – (17) become,

$$\begin{aligned} &(1+N)f'''' + ff'' - \frac{2m}{m+1}(f')^2 - N\delta\left(\frac{m+1}{2}\right)f''''(f'')^2 + \frac{2m}{m+1}A^2 - \\ &\frac{2}{m+1}M^2\sin^2\gamma(f'-A) + \frac{2}{m+1}\lambda(\theta + Nc\chi - Nr\phi) = 0, \end{aligned} \quad (18)$$

$$\theta'' + \Pr\left(+ f\theta' + Nb\,\theta'\phi' + Nt\left(\theta'\right)^2 + Nd\,\chi''\right) + \frac{2}{m+1}\left(A^* f' + B^*\theta\right) = 0, \tag{19}$$

$$\chi'' + Scf\,\chi' + Ld\,\theta'' = 0, \tag{20}$$

$$\phi'' + Sc_n f\,\phi' + \frac{Nt}{Nb}\theta'' = 0. \tag{21}$$

$$\left.\begin{aligned} &f(0) = \Omega\frac{1-m}{1+m},\ f'(0) = 1,\ \theta(0) = 1,\ \phi(0) = 1,\ \chi(0) = 1, \\ &f'(\infty) = A,\ \theta(\infty) = 0,\ \phi(\infty) = 0,\ \chi(\infty) = 0. \end{aligned}\right\} \tag{22}$$

The parameters are defined as:

$$\left.\begin{aligned} &\lambda = \frac{G_T}{\mathrm{Re}_x^2},\ G_T = \frac{(1-C_\infty)\beta_T\, g\,(T_w - T_\infty)(x+b)^3}{\upsilon^2},\ \mathrm{Re}_x = \frac{U_w(x+b)}{\upsilon},\ Nc = \frac{\beta_{C_1}(C_{1w} - C_{1\infty})}{\beta_T(T_w - T_\infty)}, \\ &Nr = \frac{(\rho_p - \rho_f)(C_w - C_\infty)}{\rho_f\,\beta_T(1-C_\infty)(T_w - T_\infty)},\ \delta = \frac{{U_0}^3(x+b)^{3m-1}}{2\upsilon {c_*}^2},\ A = \frac{U_1}{U_0},\ M^2 = \frac{\sigma {B_0}^2}{\rho_f U_0},\ U_e(x) = U_1(x+b)^m, \\ &Nb = \frac{\tau D_B(C_w - C_\infty)}{\upsilon},\ Nt = \frac{\tau D_T(T_w - T_\infty)}{\upsilon T_\infty},\ Nd = \frac{D_{TC_1}(C_{1w} - C_{1\infty})}{\upsilon(T_w - T_\infty)},\ Sc_n = \frac{\upsilon}{D_B},\ Sc = \frac{\upsilon}{D_{S_1}}, \\ &Ld = \frac{D_{C_1T}(T_w - T_\infty)}{D_{S_1}(C_{1w} - C_{1\infty})},\ \Pr = \frac{\upsilon}{\alpha},\ \upsilon = \frac{\mu}{\rho_f},\ N = \frac{1}{\mu\beta c_*}. \end{aligned}\right\} \tag{23}$$

Where C_f is given as,

$$C_f = \frac{\tau_w}{\rho_f {U_w}^2}, \tag{24}$$

Where τ_w is given as,

$$\tau_w = \left[\left(\mu + \frac{1}{\beta c_*}\right)\frac{\partial u}{\partial y} - \frac{1}{6\beta {c_*}^3}\left(\frac{\partial u}{\partial y}\right)^3\right]_{y = E(x+b)^{\frac{1-m}{2}}}. \tag{25}$$

Dimensionless expression for the skin friction coefficient we have,

$$C_f\,\mathrm{Re}_x^{\frac{1}{2}} = \sqrt{\frac{m+1}{2}}\left[(1+N)\,f''(0) - \left(\frac{m+1}{2}\right)\frac{N\delta}{3}\left(f''(0)\right)^3\right]_{y=0}. \tag{26}$$

3. METHOD OF SOLUTION:

The reduced governing equations (18) - (21) with (22) are resolved by utilizing DTM method. It is a semi-analytical technique, which can be used to calculate the nonlinear problems. Now by using DTM, we can find the solution of above equations (18) - (21) with boundary conditions (22) as follows:

$$(e+2)(1+N)(e+1)(e+3)H(e+3)+\sum_{z=0}^{e}(e+1)H(e-z)(e+2)H(z+2)-$$
$$\frac{2m}{m+1}\sum_{z=0}^{e}(e+1)(e-z+1)H(z+1)H(e-z+1)-$$
$$\frac{2}{m+1}M^2Sin^2\gamma\left((e+1)H(e+1)-A\right)+ \qquad (27)$$
$$\frac{2m}{m+1}A^2+\frac{2}{m+1}\lambda\left(G(e)+NcQ(e)-NrP(e)\right)-$$
$$\left(N\left(\frac{m+1}{2}\right)\delta\sum_{z=0}^{e}\sum_{g=0}^{z}(g+1)(g+2)H(g+2)(z-g+1)(z-g+2)\right)=0,$$
$$H(z-g+2)(e-g+1)(e-g+2)(e-g+3)H(e-g+3)$$

$$(e+1)(e+2)G(e+2)+\Pr\left(\begin{array}{l}\sum_{z=0}^{e}(z+1)G(z+1)H(e-z)+\\ Nb\sum_{z=0}^{e}(z+1)(e-z+1)P(z+1)G(e-z+1)+\\ Nt\sum_{z=0}^{e}(z+1)(e-z+1)G(z+1)G(e-z+1)+\\ Nd(e+1)(e+2)Q(e+2)\end{array}\right)+ \qquad (28)$$
$$\frac{2}{m+1}\left(A^*(e+1)H(e+1)+B^*G(e)\right)=0,$$

$$(e+1)(e+2)Q(e+2)+Sc\sum_{z=0}^{e}(z+1)Q(z+1)H(e-z)+Ld(e+1)(e+2)G(e+2)=0, \qquad (29)$$

$$(e+1)(e+2)P(e+2)+Sc_n\sum_{z=0}^{e}(z+1)P(z+1)H(e-z)+\frac{Nt}{Nb}(e+1)(e+2)G(e+2)=0. \qquad (30)$$

The boundary conditions that have been transformed are:

$$H(0)=\frac{\Omega(1-m)}{(1+m)},\ H(1)=1,\ H(2)=\frac{n_1}{2},\ G(0)=1,\ G(1)=n_2, \qquad (31a)$$

$$Q(0)=1,\ Q(1)=n_4,\ P(0)=1,\ P(1)=n_3. \qquad (31b)$$

Differential transform of $f(\xi),\ \theta(\xi),\ \chi(\xi)$ and $\phi(\xi)$ are $H(e),\ G(e),\ Q(e)$ and $P(e)$ also with the help of boundary conditions, that is, equation (22), we can find constants $n_1,\ n_2,\ n_3$ and n_4. By utilizing transformed boundary conditions (31a), (31b) and equations (27) - (30), we obtain the closed form of solution.

4. RESULT AND DISCUSSION:

To illustrate the characteristics of the problem, findings are detailed in figures 2-24. Coefficient of skin friction ($f''(0)$) on m is matched with the previous studies and present studies are shown in Table 1.

Table1. Comparison of $f''(0)$ with [15] and [12] when $N=\delta=M^2=A=\lambda=Nc=Nr=\beta=0$ and $\Omega=0.5$

m	$-f''(0)$ [15],[12]	Present study
-1/3	1.0000	1.03923
-0.5	1.1667	1.1985
-0.51	1.1859	1.1918992
-0.55	1.2807	1.2920254

4.1 Velocity profile:

Velocity degrades as values of fluid parameter δ rises is shown in Fig.2. Physically upon increasing δ, viscous force of the fluid enhances. As viscous force of the fluid enhances the velocity of the fluid diminishes. Where, in Fig. 3 the velocity rises as values of N rises. Physically upon increasing N, viscous force of the fluid diminishes. As viscous force of the fluid, decline the velocity of the fluid increases. Fig.4 captures the effects of mixed convection parameter λ on the velocity. Higher values of λ give the stronger buoyancy effects to increase the velocity. In Fig.5 velocity decreases as values of power index m rises.. It is seen that the large values of t m thins the momentum boundary layer thickness. In Fig. 6, velocity decreases as wall thickness parameter Ω increases. We can observe that as Ω increases the velocity distribution and momentum boundary layer thickness reduces for $m<1$. As values of Ω rise, the stretching velocity decreases and as a result velocity distribution decreases.Fig.7 shows that f' reduces with the rise of values of magnetic parameter M . The Lorentz force is created by applying the uniform magnetic field normal to the flow direction. The fluid in the boundary layer has a propensity to move more slowly under the influence of this force. Consequently, f' reduces when M is increased. In Fig.8, as values of an aligned angle γ rises f' reduces. Since, M is directly proportional to $Sin^2\gamma$ and there is no effect of magnetic field on velocity curves when $\gamma=0^0$ while the magnetic field effect the flow when $\gamma=90^0$. Fig.9 shows that velocity reduces as buoyancy ratio parameter Nr rises. As Nr rises the velocity boundary layer thickness rises. Hence velocity reduces. Fig. 10 shows that velocity enhances as Nc enhances. As Nc enhances the velocity boundary layer thickness decreases. Hence velocity enhances. Fig.11 explains the impact of velocity ratio parameter A on f' . A isdefined as the ratio of free stream velocity to the velocity of the stretching sheet. When $U_e(x)$ exceeds $U_w(x)$, the flow velocity rises and also the boundary layer thickness reduces as A rises. Moreover, when $U_e(x)<U_w(x)$, the flow field velocity and boundary layer thickness also increases. The boundary layer flow is inverted for $A<1$.

4.2 Temperature profile:

In Figs. 12and 13 temperature profile increases, as values of heat source sink parameters A^* and B^* increases. The reason behind is that the positive values of A^* and B^* generates the heat and generated heat increases width of the thermal boundary layer. Opposite behaviour can be seen for negative values of A^* and B^*. In Fig.14, it is visible that the impact of m is to enhance the temperature with its rise and the effects of m are more notable for shear thinning fluid.Fig.15 show that temperature profile decreases as Prandtl number $\Pr$ increases. Physically, an increase

in the value of $\Pr$, the thermal boundary layer grows thinner. Since, $\Pr$ represents is the ratio of momentum diffusivity to thermal diffusivity. $\Pr$ aids in the acceleration of cooling in conducting flows.

4.3 Solutal concentration profile:

Fig.16 indicates the change in Schmidt number Sc on solute concentration. As values of Sc rises, the solute concentration profile reduces. Sc and diffusivity of mass are inversely proportional to each other. So, higher values of Sc gives poor diffusivity of mass due to which $\chi(\eta)$ decreases. In Fig. 17, as values of Ω increases, the solute concentration distribution decreases. Same effect can be observed in Figs. 18 and 19, as A^* and B^* rises, $\chi(\eta)$ reduces. Fig.20 show that as values of m enhances the solute concentration profile decreases.

4.4 Nanoparticle concentration profile:

Fig. 21 shows that as values of Sc_n rises the nanoparticle concentration profile reduces. So, for higher values of Sc_n, the thickness of thermal boundary layer is larger than that of nanoparticle boundary layer. Fig.22 indicates that as Prandtl number $\Pr$ increases, nanoparticle concentration profile decreases. Actually, $\Pr$ is inversely related to thermal diffusivity and hence, it decreases nanoparticle concentration profile. Figs. 23 and 24 are plotted to the effect of A^* and B^* on nanoparticle concentration it is observed that concentration of fluid reduces for increase values of the parameters.

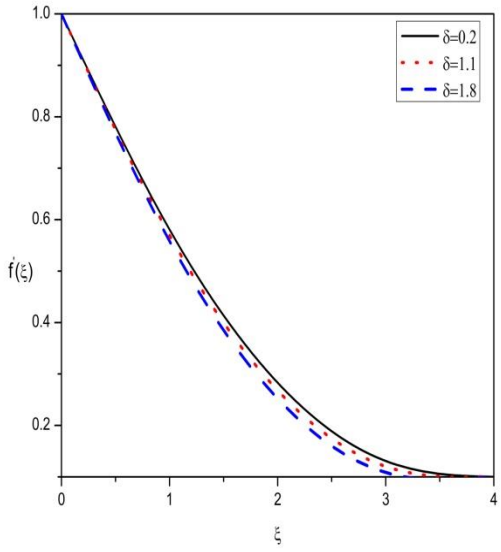

Fig. 2 Variation of $f'(\xi)$ on δ when

$M = 0.3, m = 0.5, \Omega = 0.35, \lambda = 0.44,$

$Nc = 0.2, Nr = 0.2, \gamma = \pi/4, A = 0.1, N = 0.3.$

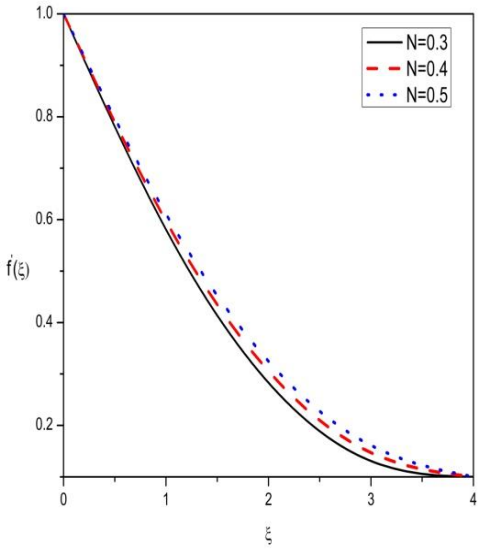

Fig. 3Variation of $f'(\xi)$ on N when

$M = 0.3, \delta = 0.2, m = 0.5, \Omega = 0.35, \lambda = 0.44,$

$Nc = 0.2, Nr = 0.2, \gamma = \pi/4, A = 0.1, N = 0.3.$

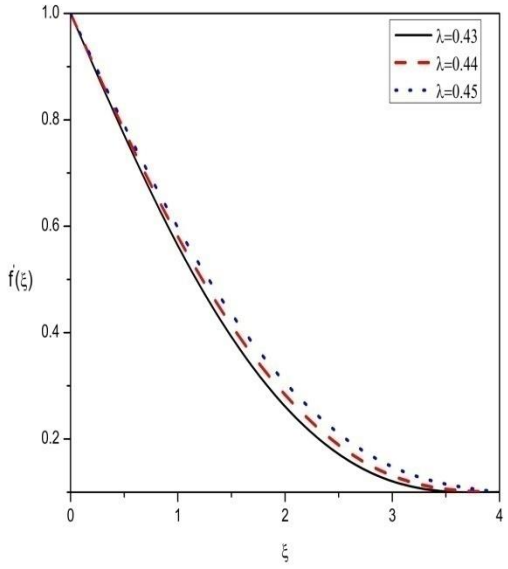

Fig. 4 Variation of $f'(\xi)$ on λ when

$M = 0.3, \delta = 0.2, m = 0.5, \Omega = 0.35, N = 0.3,$

$Nc = 0.2, Nr = 0.2, \gamma = \pi/4, A = 0.1.$

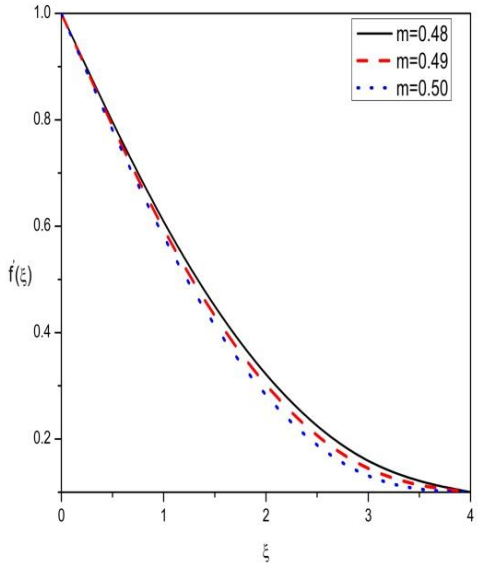

Fig. 5 Variation of $f'(\xi)$ on m when

$M = 0.3, \delta = 0.2, \lambda = 0.44, \Omega = 0.35, N = 0.3,$

$Nc = 0.2, Nr = 0.2, \gamma = \pi/4, A = 0.1.$

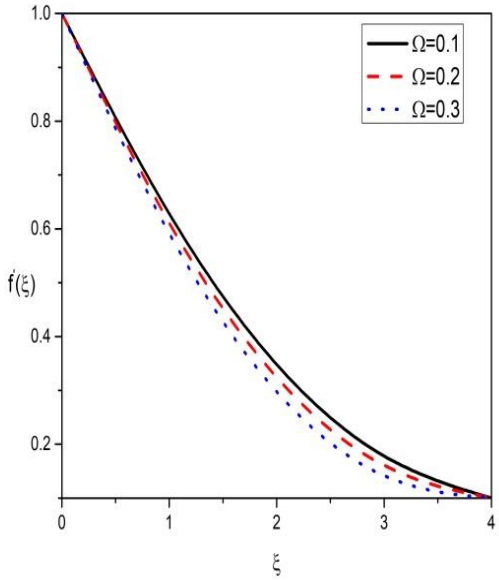

Fig. 6 Variation of $f'(\xi)$ on Ω when

$M = 0.3, \delta = 0.2, \lambda = 0.44, m = 0.5, N = 0.3,$

$Nc = 0.2, Nr = 0.2, \gamma = \pi/4, A = 0.1.$

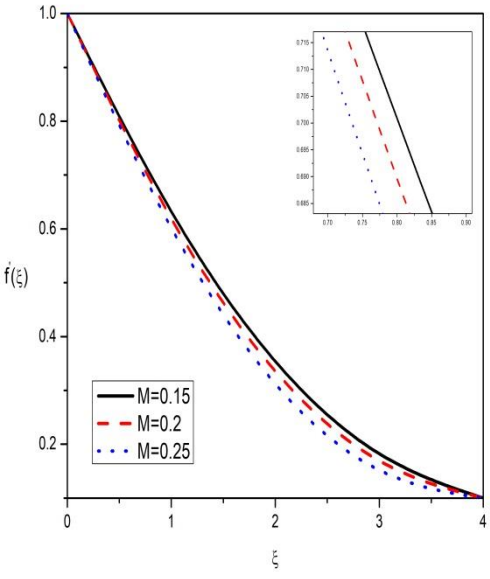

Fig. 7 Variation of $f'(\xi)$ on M when

$\Omega = 0.35, \delta = 0.2, \lambda = 0.44, m = 0.5, N = 0.3,$

$Nc = 0.2, Nr = 0.2, \gamma = \pi/4, A = 0.1.$

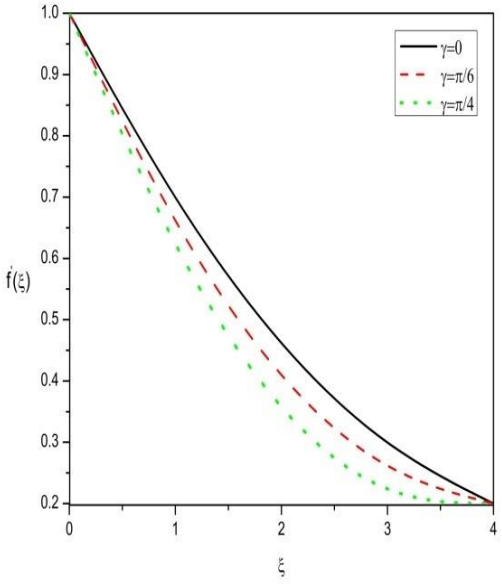

Fig. 8 Variation of $f'(\xi)$ on γ when

$\Omega = 0.35, \delta = 0.2, \lambda = 0.44, m = 0.5, N = 0.3,$

$M = 0.3, Nc = 0.2, Nr = 0.2, A = 0.1.$

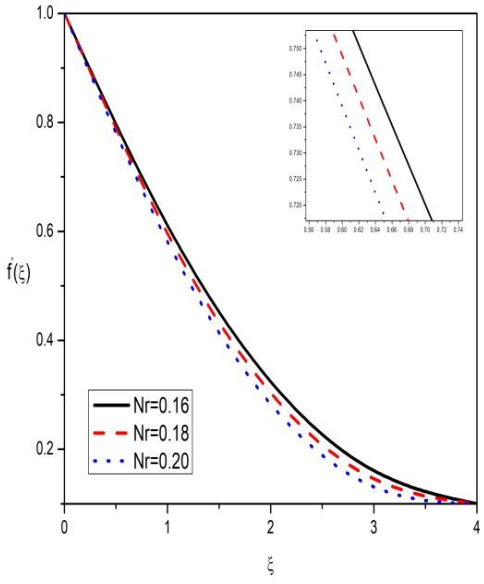

Fig. 9 Variation of $f'(\xi)$ on Nr when

$\Omega = 0.35, \delta = 0.2, \lambda = 0.44, m = 0.5, N = 0.3,$

$M = 0.3, Nc = 0.2, \gamma = \pi/4, A = 0.1.$

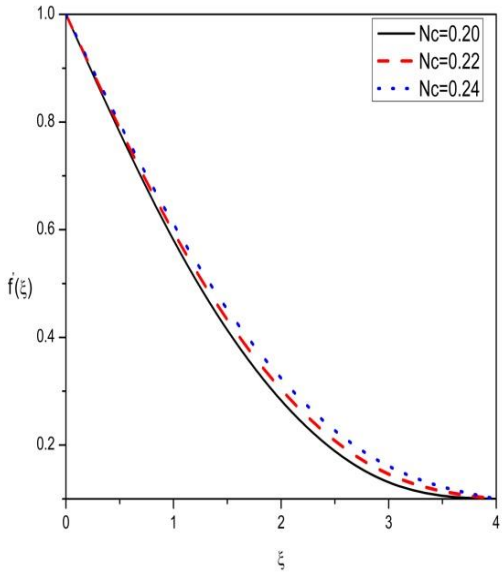

Fig. 10 variation of $f'(\xi)$ on Nc when

$\Omega = 0.35, \delta = 0.2, \lambda = 0.44, m = 0.5, N = 0.3,$

$Nr = 0.2, \gamma = \pi/4, M = 0.3, A = 0.1.$

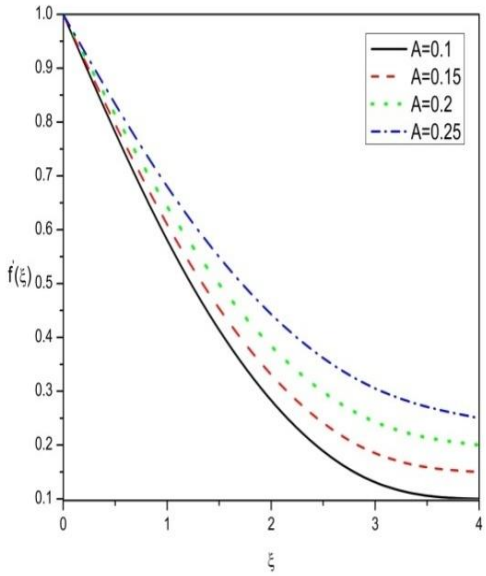

Fig.11 Variationof $f'(\xi)$ on A when

$\Omega = 0.35, \delta = 0.2, \lambda = 0.44, m = 0.5, N = 0.3,$

$Nr = 0.2, Nc = 0.2, \gamma = \pi/4, M = 0.3.$

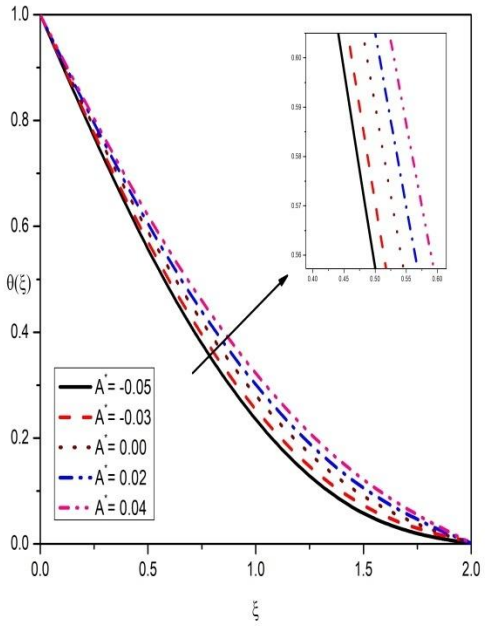

Fig. 12 Variation of $\theta(\xi)$ on A^* when

$\Omega = 0.4, \Pr = 6, Nd = 0.1, Ld = 1, Sc = 0.1,$

$Nt = 0.1, m = 0.5, Nb = 0.1, Sc_n = 0.1, B^* = 0.01.$

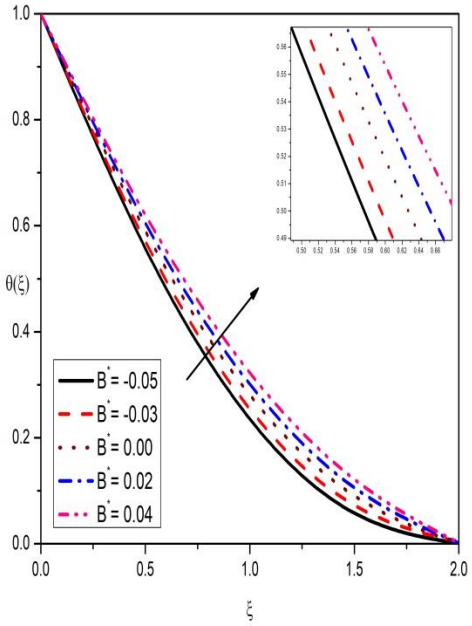

Fig. 13 Variation of $\theta(\xi)$ on B^* when

$\Omega = 0.4, \Pr = 6, Nd = 0.1, Ld = 1, Sc = 0.1,$

$Nt = 0.1, m = 0.5, Nb = 0.1, Sc_n = 0.1, A^* = 0.01.$

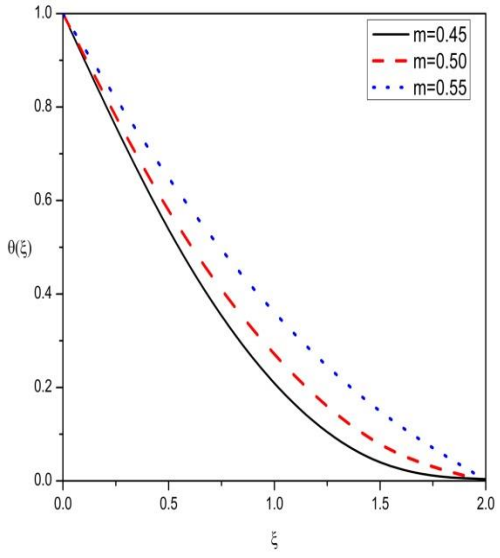

Fig. 14 Variation of $\theta(\xi)$ on m when

$\Omega = 0.4, Nd = 0.1, Ld = 1, Sc = 0.1, \Pr = 6,$

$Nt = 0.1, B^* = 0.01, Sc_n = 0.1, A^* = 0.01, Nb = 0.1.$

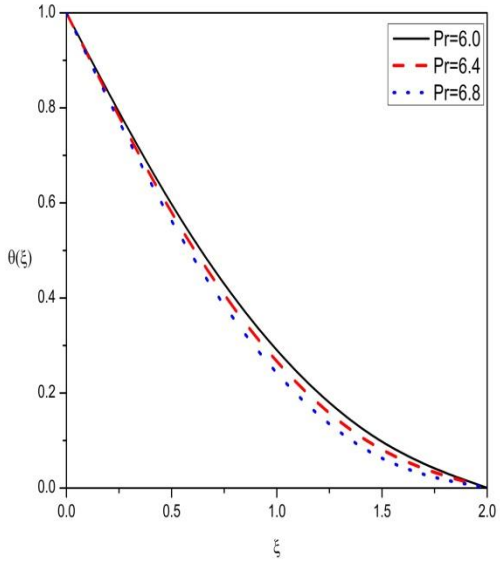

Fig. 15 Variation of $\theta(\xi)$ on $\Pr$ when

$Sc = 0.1, Ld = 1, \Omega = 0.4, m = 0.5, Nd = 0.1,$

$Nt = 0.1, B^* = 0.01, Sc_n = 0.1, A^* = 0.01, Nb = 0.1.$

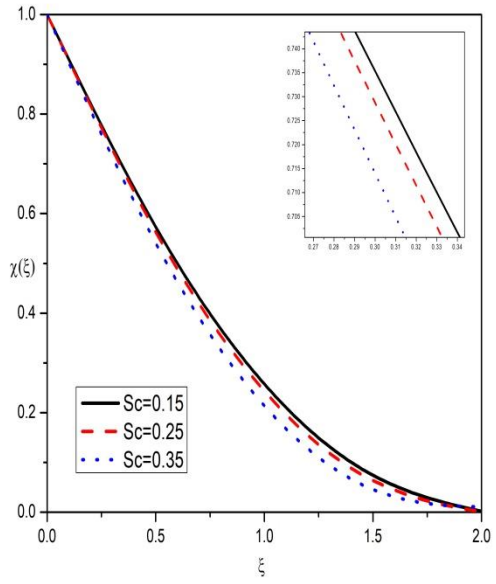

Fig. 16Variation of $\chi(\xi)$ on Sc when

$\Pr = 1, Ld = 1, m = 0.5, Nt = 2, \Omega = 0.3,$

$B^* = 0.17, Nb = 1, Ld = 1, A^* = 0.17, Nd = 0.1.$

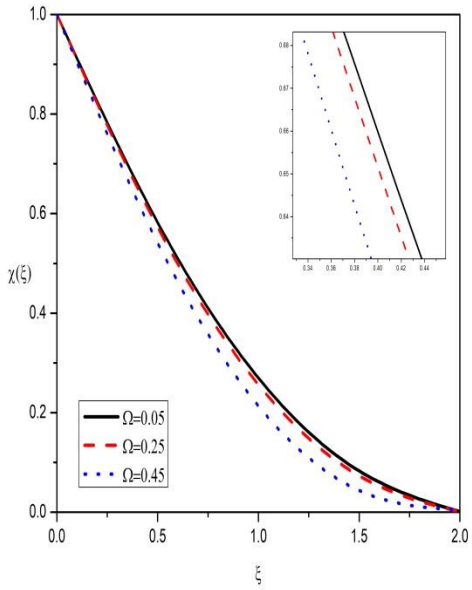

Fig.17 Variation of $\chi(\xi)$ on Ω when

$\Pr = 1, Ld = 1, m = 0.5, Nt = 2, Sc = 0.2,$

$B^* = 0.17, Nb = 1, Sc = 0.2, A^* = 0.17, Nd = 0.1.$

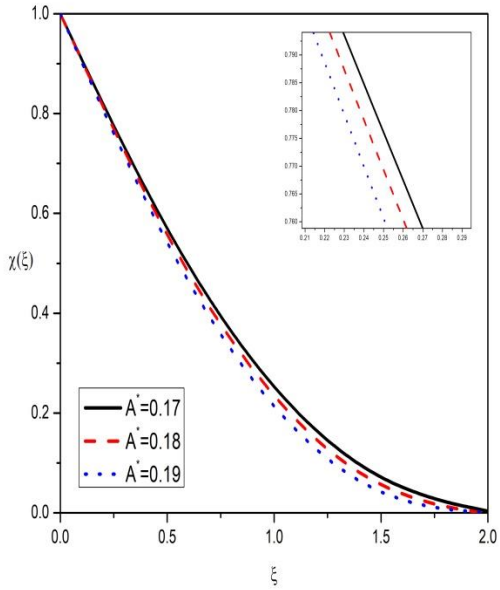

Fig. 18 Variation of $\chi(\xi)$ on A^* when

$\Pr = 1, Ld = 1, Nd = 0.1, \Omega = 0.3, B^* = 0.17,$

$Nb = 1, m = 0.5, Sc = 0.2, Nt = 2.$

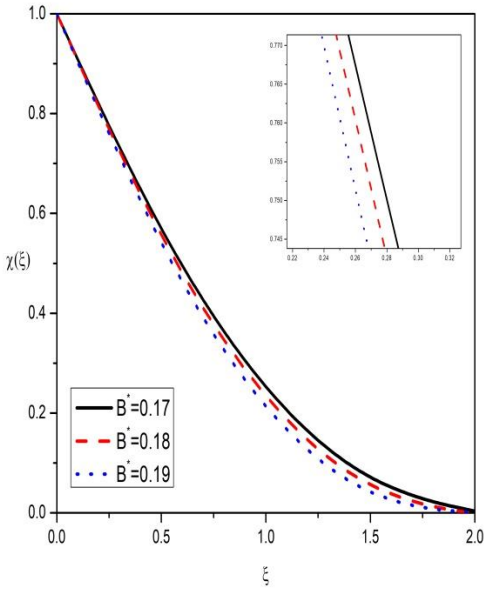

Fig.19Variation of $\chi(\xi)$ on B^* when

$\Pr = 1, Ld = 1, Nd = 0.1, \Omega = 0.3, A^* = 0.17,$

$Nb = 1, m = 0.5, Sc = 0.2, Nt = 2.$

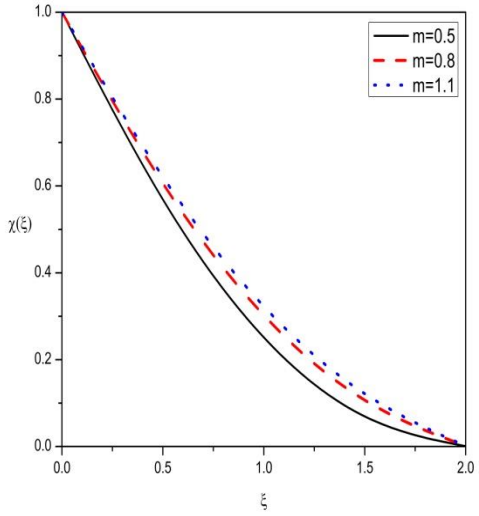

Fig. 20 Variation of $\chi(\xi)$ on m when

$\Pr = 1, Ld = 1, B^* = 0.17, Nt = 2, Sc = 0.2, Nb = 1, Nd = 0.1, A^* = 0.17, \Omega = 0.3.$

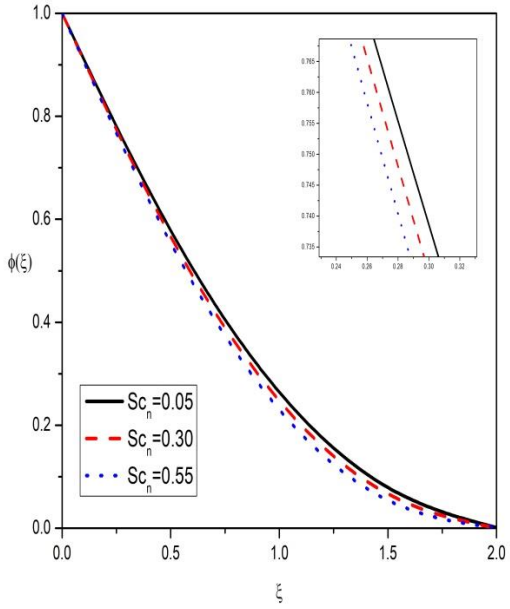

Fig. 21Variation of $\phi(\xi)$ on Sc_n when

$\Pr = 1, Ld = 1, B^* = 0.17, Nt = 0.1, m = 0.5, B^* = 0.17,$

$Nb = 0.1, Nd = 0.1, A^* = 0.17, \Omega = 0.4.$

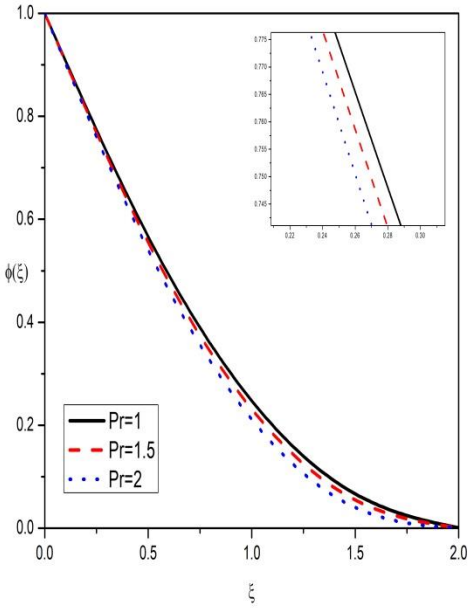

Fig. 22 Variation of $\phi(\xi)$ on Pr when

$Sc_n = 0.3, Ld = 1, B^* = 0.17, Nt = 0.1, m = 0.5,$

$Nb = 0.1, Nd = 0.1, A^* = 0.17, \Omega = 0.4.$

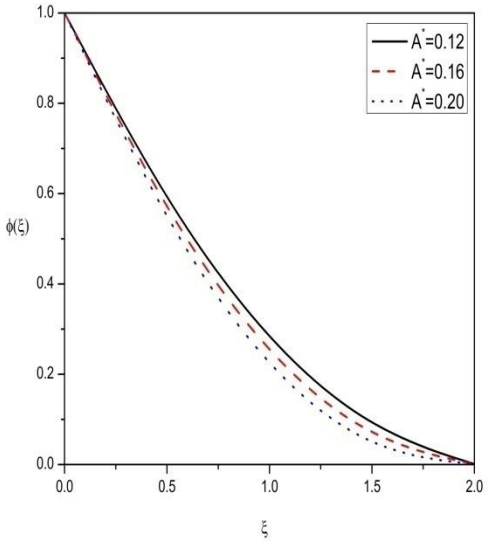

Fig. 23 Variation of $\phi(\xi)$ on A^* when $Sc_n = 0.3, Ld = 1, B^* = 0.17, A^* = 0.17, Nt = 0.1,$ $Nb = 0.1, Nd = 0.1, \Omega = 0.4, m = 0.5, \Pr = 1.$

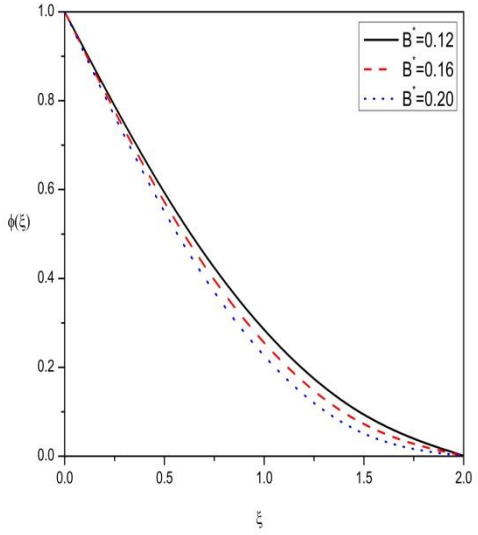

Fig. 24 Variation of $\phi(\xi)$ on B^* when $Sc_n = 0.3, Ld = 1, A^* = 0.17, Nt = 0.1, B^* = 0.17,$ $Nb = 0.1, Nd = 0.1, \Omega = 0.4, m = 0.5, \Pr = 1.$

5. CONCLUSIONS:

The present work analyzes the double diffusive mixed convection stagnation point flow over a slender stretching sheet including an inclined magnetic field and non-uniform heat source sink. The main observations are given below:

- The velocity profile shows opposite behaviour with δ and N .
- It is noticed that λ gives the stronger buoyancy effects to enhance the velocity profile and γ the deduces the velocity profile. Also γ impacts the magnetic field on velocity curves when $\gamma = 90^0.$
- A^* and B^* improves the heat generation, whereas it degrades the solutal, nanoparticle concentration profiles.
- Rise in the momentum boundary layer thickness and a decrease in thermal boundary layer thickness were noted for the rising values of the power index parameter m including shear thinning to shear thickening fluids.

REFERENCES:

1. Crane,L. J. (1970). Flow past a stretching plate, *Journal of Applied Mathematics and Physic*s,*21,* 645–647.
2. Salleh, M. Z., Nazar, R., & Pop, I. (2010). Boundary layer flow and heat transfer over a stretching sheet with Newtonian heating. *Journal of the Taiwan Institute of Chemical Engineers, 41(6),* 651–655.
3. Farooq, M., Khan, M. I., Waqas, M., Hayat, T., Alsaedi, A., & Khan, M. I. (2016). MHD stagnation point flow of viscoelastic nanofluid with non-linear radiation effects. *Journal of Molecular Liquids, 221,* 1097–1103.

4. Yao, S., Fang, T., &Zhong, Y. (2011). Heat transfer of a generalized stretching/shrinking wall problem with convective boundary conditions.*Communications in Nonlinear Science and Numerical Simulation, 16(2),* 752–760.
5. Vajravelu, K. (2001).Viscous flow over a nonlinearly stretching sheet. *Applied Mathematics and Computation, 124,* 281–288.
6. Ishak, A., Nazar, R., & Pop, I. (2008). Hydromagnetic flow and heat transfer adjacent to a stretching vertical sheet*. Heat Mass Transfer, 44(8),* 921–927.
7. Hsiao, K.L. (2013). Energy conversion conjugate conduction–convection and radiation over non-linearly extrusion stretching sheet with physical multimedia effects. *Energy, 59,* 494–502.
8. Bhattacharyya, K., &Vajravelu, K. (2012). Stagnation-point flow and heat transfer over an exponentially shrinking sheet. *Communications in Nonlinear Science and Numerical Simulation, 17(7),* 2728–2734*.*
9. Seini, Y. I., &Makinde, O. D. (2013). MHD Boundary Layer Flow due to Exponential Stretching Surface with Radiation and Chemical Reaction. *Mathematical Problems in Engineering, 2013,* 1–7.
10. Elbashbeshy, E. M. A. (2001). Heat transfer over an exponentially stretching continuous surface with suction. *Achieves of Mechanics, 53(6),*643-651.
11. Lee, L. L. (1967). Boundary layer over a thin needle. *The physics of fluids, 10*, 820-822.
12. Fang, T., Zhang, J., &Zhong, Y. (2012) Boundary Layer Flow over a Stretching Sheet with Variable Thickness. *Applied Mathematics and Computation, 218,* 7241-7252.
13. Khader, M. M., &Megahed, A. M. (2013). Numerical solution for boundary layer flow due to a nonlinearly stretching sheet with variable thickness and slip velocity*. The European Physical Journal Plus, 128(9*),100.
14. Reddy C, S., Naikoti, K., &Rashidi, M. M. (2017). MHD flow and heat transfer characteristics of Williamson nanofluid over a stretching sheet with variable thickness and variable thermal conductivity. *Transactions of A. Razmadze Mathematical Institute, 171(2),* 195–211.
15. Hayat, T., Bashir, Z., Qayyum, S., &Alsaedi, A. (2017). Investigation of double diffusion Cattaneo-Christov model in mixed convection flow by variable thickness surface. *Results in Physics, 7,* 3873–3881*.*
16. Mahapatra, T. R., & Gupta, A. S. (2002). Heat transfer in stagnation-point flow towards a stretching sheet. *Heat and Mass Transfer, 38(6),* 517–521.
17. Rehmana, A.,Achakzai, S., Nadeem,S., &Iqbal, S. (2016). Stagnation point flow of Eyring Powell fluid in a vertical cylinder with heat transfer. *Journal of Power Technologies, 96,* 57–62.
18. Rehman, A., & Sheikh,N. (2017). Boundary Layer Stagnation-Point Flow of Micropolar Fluid over an Exponentially Stretching Sheet.*International Journal of Fluid Mechanics & Thermal Sciences, 3,* 25-31.
19. VinodKumar,G., Kiran Kumar, R. V. M. S. S., &Varma, S. V. K. (2018). Unsteady Magnetohydrodynamic Stagnation Point Flow of a Nanofluid over a Slendering Stretching Sheet using Buongiorno's Model. *International Journal of Research in Industrial Engineering, 7,* 84–105.

20. Seth, G. S., &Mandal, P. K. (2019). Analysis of Electromagnetohydrodynamic Stagnation Point Flow of Nanofluid Over a Nonlinear Stretching Sheet with Variable Thickness. *Journal of Mechanics, 35,*719–733.
21. Agbaje, T. M., Mondal, S., Makukula, Z. G., Motsa, S. S., &Sibanda, P. (2018). A new numerical approach to MHD stagnation point flow and heat transfer towards a stretching sheet. *Ain Shams Engineering Journal, 9(2),* 233–243.
22. Tlili,I.,Khan, W. A.,&Ramadan, K. (2018). Entropy Generation Due to MHD Stagnation Point Flow of a Nanofluid on a Stretching Surface in the Presence of Radiation.*Journal of Nanofluids, 7,* 879–890.
23. Bhuvanavijaya,R.,&Mallikarjuna,B. (2013).Double Diffusive Convection of a Rotating Fluid Over a VerticalPlate Embedded in Darcy-Forchheimer Porous Medium with Non-Uniform Heat Sources*.International Journal of Emerging Trends in Engineering and Development, 2,* 415-432.
24. Venkateswarlu,S.,Varma, S.V.K.,&Kiran Kumar, R.V.M.S.S. (2018). Thermo-diffusion and non-uniform heat source/sink effects on hydromagnetic flow of Cu and TiO2 water - based nanofluid partially filled with a porous medium.*Informatics in Medicine Unlocked, 13*, 51-61.
25. Sugunamma,V.,Ramana Reddy, J.V.,Sandeep,N.,&Anantha Kumar,K. (2016). Influence of non uniform heat source/sink on MHD nanofluid flow past MHD nanofluid flow past a slendering stretching sheet with slip effects, *Global Journal of Pure and Applied Mathematics,12.*
26. Hayat, T., Ullah, I., Alsaedi, A., &Farooq, M. (2017). MHD flow of Powell-Eyring nanofluid over a non-linear stretching sheet with variable thickness. *Results in Physics, 7,* 189–196.
27. Abdul Halim, N., &Mohd Noor, N. F. (2021). Mixed Convection Flow of Powell–Eyring Nanofluid near a Stagnation Point along a Vertical Stretching Sheet. *Mathematics, 9(4),* 364.
28. Kotnurkar, A., &Giddaiah, S. (2018). Mixed Convection Peristaltic Flow of aEyring-Powell Nanofluid with Magnetic Field in a Non-Uniform Channel.*Journal of Applied Mathematics and Computation, 2,* 332-344.
29. Rasool, G., &Shafiq, A. (2020). Numerical exploration of the features of thermally enhanced chemically reactive radiative Powell–Eyring nanofluid flow via Darcy medium over non-linearly stretching surface affected by a transverse magnetic field and convective boundary conditions. *Applied Nanoscience.*doi: https://doi.org/10.1007/s13204-020-01625-2.
30. Sepasgozar, S.,Faraji,M., &Valipour,P. (2017). Application of differential transformation method for heat and mass transfer in a porous channel.*Propulsion and Power Research, 6,* 41-48.
31. Mirzaaghaian, A., &Ganji, D. D. (2016). Application of differential transformation method in micropolar fluid flow and heat transfer through permeable walls. *Alexandria Engineering Journal, 55(3),* 2183–2191.
32. Hatami,M., &Jing, D. (2016). Differential transformation method for Newtonian and non-Newtonian nanofluids flow analysis: compared to numerical solution.*Alexandria Engineering Journal, 55(2),* 731-739

APPENDIX

Let us take a function $f(\xi)$ that is analytical in a domain D and let $\xi=\xi_0$ any pointed noted in D. The function $f(\xi)$ is then expressed by a power series with center isplaced at ξ_0. The differential transform of the function $f(\xi)$ for e^{th} derivative of is,

$$F(e)=\frac{1}{e!}\left[\frac{d^e f(\xi)}{d\xi^e}\right]_{\xi=\xi_0}, \tag{32}$$

Here, $f(\xi)$ gives the original function and $F(e)$ is transformed function. The inverse differential transform is,

$$f(\xi)=\sum_{e=0}^{\infty}F(e)(\xi-\xi_0)^e, \tag{33}$$

In real applications, the function $f(\xi)$ is expressed by a finite series and eq. (33) can be written as

$$f(\xi)=\sum_{e=0}^{b}F(e)(\xi-\xi_0)^e, \tag{34}$$

Eq. (34) implies that $f(\xi)=\sum_{e=b+1}^{\infty}F(e)(\xi-\xi_0)^e$, is negligibly small. In fact, b is series size in this problem. Some of the basic properties of DTM are shown in Table 2.

Table 2: The basic properties of DTM

Original function	Transformed function
$f(\xi)=a(\xi)\pm b(\xi)$	$F(e)=A(e)\pm B(e)$
$f(\xi)=c.a(\xi)$	$F(e)=c.A(e)$, c is a constant
$f(\xi)=\frac{d^n a(\xi)}{d\xi^n}$	$F(e)=(e+1)(e+2)(e+3).....(e+n)A(e+n)$
$f(\xi)=a(\xi)\frac{db(\xi)}{d\xi}$	$F(e)=\sum_{z=0}^{e}(z+1)A(e-z)B(z+1)$
$f(\xi)=\frac{da(\xi)}{d\xi}\frac{db(\xi)}{d\xi}$	$F(e)=\sum_{z=0}^{e}(z+1)(e-z+1)A(z+1)B(e-z+1)$
$f(\xi)=\xi^n$	$F(e)=\delta(e-z)=\begin{cases}1 & if\ e=n\\ 0 & if\ e\neq n\end{cases}$

Differential transform of $f(\xi),\ \theta(\xi),\ \chi(\xi)$ and $\phi(\xi)$ are $H(e),\ G(e),\ Q(e)$ and $P(e)$ also with the help of boundary conditions, that is, equation (22), we can find constants $n_1,\ n_2,\ n_3$ and n_4. By using Eq. (31a) and (31b) we get the following iterations.

$$H(0)=\frac{\Omega(1-m)}{(1+m)},\quad H(1)=1,\qquad H(2)=\frac{n_1}{2},$$

$$H(3)=\frac{1}{6\left(1+N-N\delta n_1^{\,2}\left(\frac{1+m}{2}\right)\right)}\left[\frac{2m}{1+m}-\frac{n_1(1-m)\Omega}{1+m}+\frac{2M^2\sin^2(\gamma)(1-A)}{1+m}-\frac{2mA^2}{1+m}-\frac{2\lambda(Nc-Nr+1)}{1+m}\right],\text{ ---so on.}$$

$$G(0)=1,\quad G(1)=n_2,$$

$$G(2)=\frac{1}{(2-2Ld\,\mathrm{Pr}\,Nd)}\left[-\frac{(1-m)\Omega\,\mathrm{Pr}\,n_2}{1+m}-\mathrm{Pr}\,Nbn_2n_3-\mathrm{Pr}\,Ntn_2^{\,2}+\frac{\mathrm{Pr}\,NdScn_4(1-m)\Omega}{1+m}+\frac{2\left(A^*+B^*\right)}{1+m}\right],\text{ ---so on.}$$

$$Q(0)=1,\quad Q(1)=n_4,$$

$$Q(2)=\left[-\frac{(1-m)\Omega Scn_4}{2(1+m)}-\frac{Ld\left(\frac{(1-m)\Omega\,\mathrm{Pr}\,n_2}{(1+m)}\right)-\mathrm{Pr}\,Nbn_2n_3-\mathrm{Pr}\,Ntn_2^{\,2}+\frac{\mathrm{Pr}\,NdScn_4(1-m)\Omega}{1+m}-\frac{2\left(A^*+B^*\right)}{1+m}}{(2-2Ld\,\mathrm{Pr}\,Nd)}\right],\text{ ---so on.}$$

$$P(0)=1,\quad P(1)=n_3,$$

$$P(2)=\left[-\frac{(1-m)\Omega Sc_n n_3}{2(1+m)}-\frac{Nt\left(\frac{(1-m)\Omega\,\mathrm{Pr}\,n_2}{(1+m)}\right)-\mathrm{Pr}\,Nbn_2n_3-\mathrm{Pr}\,Ntn_2^{\,2}+\frac{\mathrm{Pr}\,NdScn_4(1-m)\Omega}{1+m}-\frac{2\left(A^*+B^*\right)}{1+m}}{Nb(2-2Ld\,\mathrm{Pr}\,Nd)}\right],\text{ ---so on.}$$

Putting these iterations in Eq. (34), we obtain the following closed form of solutions.

$$f(\eta)=\frac{\Omega(1-m)}{(1+m)}+1.\eta+\frac{n_1}{2}\eta^2+\frac{1}{6\left(1+N-N\delta n_1^{\,2}\left(\frac{1+m}{2}\right)\right)}\left[\frac{2m}{1+m}-\frac{n_1(1-m)\Omega}{1+m}+\frac{2M^2\sin^2(\gamma)(1-A)}{1+m}-\frac{2mA^2}{1+m}-\frac{2\lambda(Nc-Nr+1)}{1+m}\right]\eta^3+---$$

$$\theta(\eta)=1+n_2\eta+\frac{1}{(2-2Ld\,\mathrm{Pr}\,Nd)}\left[-\frac{(1-m)\Omega\,\mathrm{Pr}\,n_2}{1+m}-\mathrm{Pr}\,Nbn_2n_3-\mathrm{Pr}\,Ntn_2^{\,2}+\frac{\mathrm{Pr}\,NdScn_4(1-m)\Omega}{1+m}+\frac{2\left(A^*+B^*\right)}{1+m}\right]\eta^2+---$$

$$\chi(\eta)=1+n_4\eta+\left[-\frac{(1-m)\Omega Scn_4}{2(1+m)}-\frac{Ld\left(\frac{(1-m)\Omega\,\mathrm{Pr}\,n_2}{(1+m)}\right)-\mathrm{Pr}\,Nbn_2n_3-\mathrm{Pr}\,Ntn_2^{\,2}+\frac{\mathrm{Pr}\,NdScn_4(1-m)\Omega}{1+m}-\frac{2\left(A^*+B^*\right)}{1+m}}{(2-2Ld\,\mathrm{Pr}\,Nd)}\right]\eta^2+---$$

$$\phi(\eta)=1+n_3\eta+\left[-\frac{(1-m)\Omega Sc_n n_3}{2(1+m)}-\frac{Nt\left(\frac{(1-m)\Omega\,\mathrm{Pr}\,n_2}{(1+m)}\right)-\mathrm{Pr}\,Nbn_2n_3-\mathrm{Pr}\,Ntn_2^{\,2}+\frac{\mathrm{Pr}\,NdScn_4(1-m)\Omega}{1+m}-\frac{2\left(A^*+B^*\right)}{1+m}}{(2-2Ld\,\mathrm{Pr}\,Nd)}\right]\eta^2+---$$